DOI: https://doi.org/10.37434/tpwj2025.04.03

APPLICATION OF MICROPLASMA DEPOSITION FOR 3D PRINTING OF AEROSPACE ENGINE PARTS

V.Yu. Khaskin[1], **K.M. Sukhyi**[2], **O.V. Ovchynnykov**[1], **O.V. Zaichuk**[2]

[1]E.O. Paton Electric Welding Institute of the NASU
11 Kazymyr Malevych Str., 03150, Kyiv, Ukraine
[2]Ukrainian State University of Science and Technologies
2 Lazaryana Str., 49010, Dnipro, Ukraine

ABSTRACT

The work is devoted to establishing the basic technological regularities and features of the formation of characteristic structures of metal layers during additive microplasma deposition with powders of corrosion- and heat-resistant alloys and determining the prospects of this process for 3D printing of aircraft parts. The work established that the choice of the mode of additive microplasma deposition of the selected group of powders is mainly determined by the size of the filler powder fraction. The energy input and thermal power of the constricted arc for growing metal products with a wall thickness of up to 3 mm using powders based on Fe and Ni with a fraction of 40–100 μm were determined. The main features of the structure formation of the metal of samples produced by microplasma deposition, and their mechanical characteristics were determined, and the tendency to burnout of alloying elements of the deposited alloy was assessed. It is shown that despite the need for finishing mechanical treatment of critical functional surfaces, the use of microplasma deposition can be considered a fairly promising direction for 3D printing of metal parts of aircraft equipment.

KEYWORDS: 3D printing, nickel alloy, microplasma deposition, metal powders, technological modes, dendritic structure, heat dissipation, mechanical properties

INTRODUCTION. ANALYSIS OF PUBLISHED DATA AND PROBLEM DEFINITION

Application of 3D printing with metallic powder materials is a promising direction in modern aerospace industry. When designing rapidly adaptable technologies of manufacturing unmanned aerial vehicles (UAV) there is the need for development of fuel-efficient and flexible technological solutions. Such products can be produced quite simply and quickly from polymer and metallic materials [1]. 3D printing technologies are the most suitable for development of such parts [2]. These technologies can be used to manufacture both the body elements and engine components [3].

To shorten the aircraft downtime during its repair, it is often necessary to apply multilevel production systems, which manufacture complex expensive components, and considerable investments into storage facilities are required, so as to ensure timely delivery of the manufactured parts [4]. Instead, the use of additive technologies allows carrying out on-site production of complex parts in good time, based on digital data without complex tools or mechanisms. Such an approach is particularly relevant for additive deposition (or 3D printing) of metal powders with manufacturing of finished metal products [5].

At present during maintenance and repair of aerospace vehicles various additive technologies are used for 3D printing of finished metal parts, in particular, supersonic particle deposition (SPD) and laser additive deposition (LAD) [6]. Such technologies are used to lower the cost of repair and maintenance, and increase the operational readiness of the vehicles. However, these technologies in themselves are rather costly in industrial application, and they also have comparatively low productivity [7]. Note that one of the main advantages of such additive technologies is the high precision of manufacturing these products. Such precision, however, is not always necessary, and in a number of cases it can be achieved by simultaneous application of additive deposition and machining [8].

One of the ways of further lowering the cost of metal 3D products with a simultaneous increase of their manufacturing productivity is application of arc methods of additive deposition of metals. In this sense, microplasma powder deposition is both interesting and promising [9]. Additive microplasma 3D printing with metal powders is an innovative technology based on welding, which allows creating parts of a relatively small size with a low cost and high productivity [10]. Such a technology enables, in particular, development of parts with functionally graded components [11] or low specific weight [12]. However, at present the 3D printing by additive microplasma powder deposition has not become widespread, because of insufficient scope of data on the rational modes of the process, which requires conducting technological research.

RESEARCH OBJECTIVE AND TASKS

The objective of the work to establish basic technological regularities and features of formation of the characteristic structures of metal layers in additive

microplasma deposition with powders of corrosion- and heat resistant alloys, based on iron and nickel, determination of the prospects of this process for 3D printing of parts of aerospace engines.

To achieve this objective, the following tasks were solved:

1. Establishing the basic technological regularities of additive microplasma deposition of powders of corrosion- and heat-resistant alloys during manufacture of 3D products.

2. Determination of the features of formation of the characteristic structures of metal layers in additive microplasma deposition of the selected alloy powders.

3. Determination of basic mechanical characteristics of the deposited metal by conducting mechanical testing of samples produced by additive microplasma deposition.

MATERIALS, EQUIPMENT AND INVESTIGATION METHODS

To achieve the objective of this study and solve the posed tasks, the following procedure was accepted:

- selection and preparation of powder filler materials for additive microplasma deposition;
- selection of the parameters of the technological mode of microplasma deposition;
- modeling the plasmatron design and flow speeds/rates of plasma-forming and shielding gases, in order to achieve a stable laminar mode of constricted plasma generation;
- creation of a laboratory stand to carry out the technological research;
- conducting experiments on deposition of spatial geometrical primitives by microplasma method with application of the selected powder filler materials;
- performance of metallographic examination of the deposited samples, determination of the characteristic defects and ways to remove them, establishing the regularities of formation of the characteristic structures of the deposited layers and prospects for application of this process for 3D printing of aircraft parts.

When producing the 3D metal objects, layer-by-layer deposition was performed on substrates from Q235 steel of 100×100×10 mm size. The compositions of the materials of the substrate and surfacing powders are given in Table 1. Corrosion-resistant powders HYF 103, 316L and PG SR2 were used to conduct preliminary research and to optimize the deposition modes, which allowed reducing the scope of experimental work with heat-resistant powders KhN50VMTYuB (EP648) and KhN60VT (VZh98). Chemical composition of powders from KhN50VMTYuB (EP648) alloy corresponded to the requirements of special technical conditions and industry standard (OST1 90126–85 and TU14-1-3046–97), powder from KhN60VT alloy (VZh98) — to TU 14-1-4296–87.

A specialized microplasma torch was developed for deposition, which will be discussed below. A disperser-feeder of an original design with a regulated range of powder flow rates G = 1.0–4.0 g/min was used for feeding the powders.

There are a number of requirements to powders used for 3D printing of parts with application of additive technologies. Among them, the following are mandatory: spherical form of the powder and size, which should not exceed 100 μm. These are exactly the powders that are the most technologically advanced, and have high bulk density, which was determined in keeping with DSTU 2640. High bulk density was indicative of compact ar-

Table 1. Chemical composition of filler powders and substrate for deposition

Material	Elemental composition, wt.%										
	Fe	B	C	Si	Mn	Ni	Cr	Cu	P	S	Others
Substrate metal											
Q235 steel	Base	–	0.14–0.22	0.05–0.15	0.4-0.65	<0.3	<0.3	<0.3	<0.04	<0.05	–
Filler (surfacing) materials											
HYF-103 powder (40–60 μm granulation)	Base	1.15	–	0.75	0.6	7.85	15.55	–	<0.02	<0.01	Mo <3.0
Powder of 316L stainless steel (40–60 μm granulation)		–	0.03	<0.6	<0.8	14–16	15–17	–	<0.02	<0.015	Mo 2.5–3.0
Powder of Ni–Cr–B–Si system (60–100 μm granulation)	<5.0	2.0–2.8	0.4–0.7	2.5–3.5	–	Base	13.5–16.5	–	<0.04	<0.04	Al <0.8
Powder KhN50VMTYuB (EP648) 40–100 μm	<4.0	0.008	<0.03	<0.04	<0.5		32–35	–	<0.010	<0.015	Nb – 0.5–1.1; Ti – 0.5–1.1; Al – 0.5–1.1; Mo – 2.3–3.3; W – 4.3–5.3
Powder KhN60VT (VZh98) 60–100 μm	<4.0	–	<0.1	<0.8	<0.5		23.5–26.5	–	<0.013	<0.013	Ti – 0.3–0.7; W – 13–16

Table 2. Results of determination of bulk density of powders from heat-resistant alloys

Data on powder	Bulk density, g/cm³	
Alloy	KhN60VT	KhN50VMTYuB
60–100	3.41	3.52
≤63	4.25	4.72

rangement of the powder particles, which is important to form products on their base. Table 2 gives the results of determination of bulk density for powders from KhN60VT (VZh98) and KhN50VMTYuB alloys (EP648). The size and fractional distribution of the studied powders were determined by sieve analysis.

Powders of a regular spherical shape were used for microplasma deposition. The size of powder particles, determined on an unetched transverse microsection, was in the range of 48–101 μm. An example of metallographic study of powder from heat-resistant nickel alloy is given in Figure 1.

To perform the deposition, preliminary preparation of filler materials was conducted, which consisted of selection of powders of a certain fractional composition, by their sieving through a set of the appropriate calibration sieves. Before calibration, the powders were preheated in a muffle furnace at the temperature of 150–200 °C to remove residual moisture, the presence of which is associated with their hygroscopicity.

Used as the microplasma power source was Tetrix 421 AC/DC (EWM GmbH Company, Germany) fitted with a plasma module with the range of current regulation of 5–50 A. Welding plasmatron of the microplasma welding unit MPU-4 (Ukraine) was selected as the base for creation of a laboratory experimen-

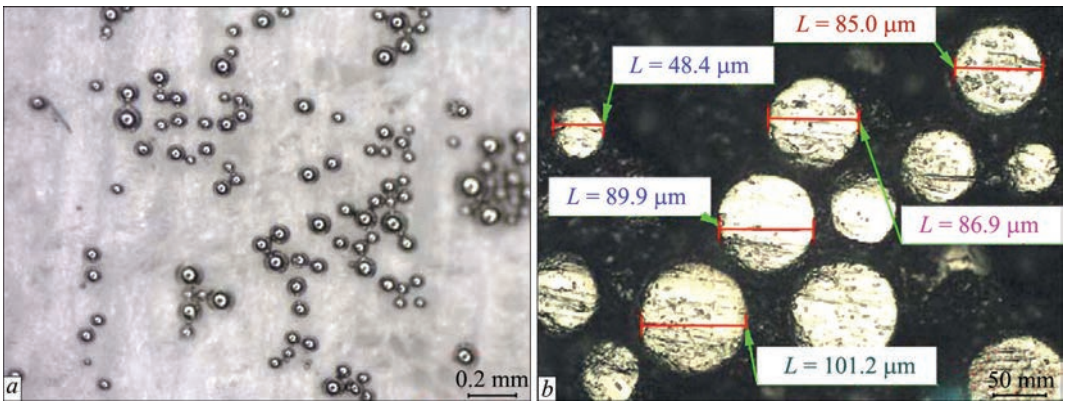

Figure 1. Powder from heat-resistant nickel alloy KhN50VMTYuB: *a* — appearance (binocular), ×40; *b* — unetched transverse section (powder embedded in Bakelite), ×200

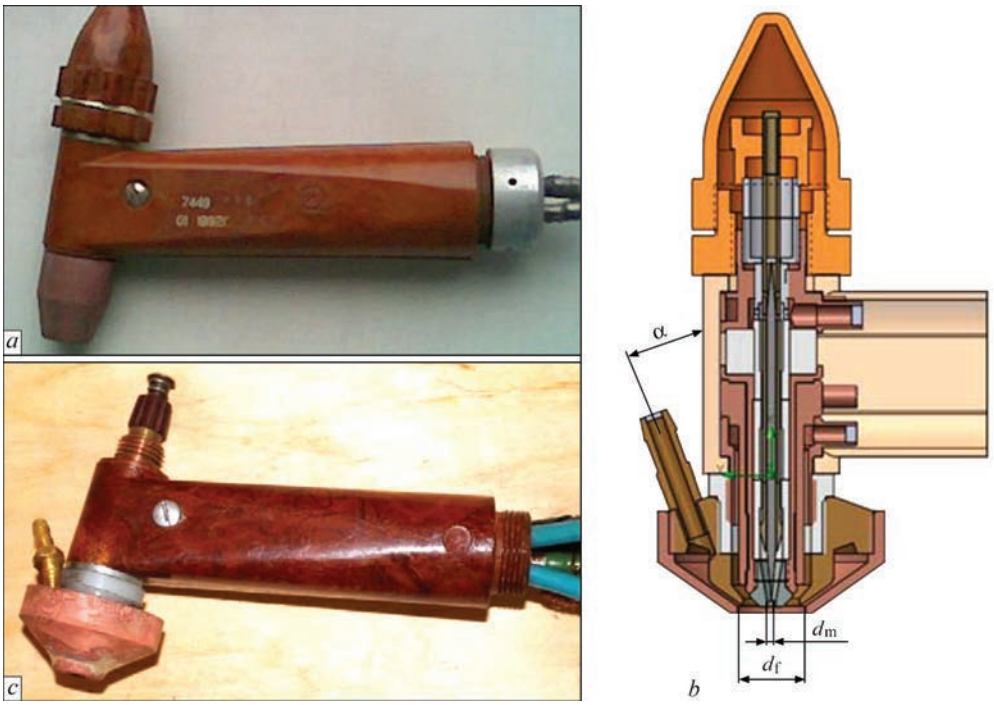

Figure 2. General view of MPU-4 plasmatron for microplasma welding (*a*), scheme of the upgraded structure (*b*) and its appearance after upgrading (*c*) with nozzle assembly for powder injection into the plasma jet (through a nipple located at an angle α ≤ 45° to plasmatron axis)

tal torch for additive deposition, which was subjected to the necessary upgrading (Figure 2). A specialized nozzle assembly was designed for powder feeding. The assembly has a system of nozzles, which allowed, in addition to protection of the deposition zone, also controlling the transporting gas with the powder relative to the plasma column coordinate. Cooling of plasmatron assemblies was also improved for its reliable operation in the range of currents of 5–100 A. The plasmatron was moved relative to the sample being surfaced, using an anthropomorphous robot-manipulator of ARC Mate 50D type (FANUC, Europe).

Computational software SolidWorks Flow Simulation was applied during design of the specialized nozzle assembly [13]. This software was used to model and optimize by the flow laminarization criterion the dynamics of plasmatron gas flows and design of the specialized nozzle assembly for powder feeding to perform additive microplasma deposition.

Table 3. Technological parameters of microplasma deposition process, used in modeling the operation of MPU-4 plasmatron with nozzle assembly for powder deposition

Number	Parameter description	Value
1	Speed of plasma-forming Ar gas flow (Q_{pl}), l/min	1.0–1.5
2	Speed of shielding Ar gas flow (Q_{sh}), l/min	10
3	Speed of transporting Ar gas flow (Q_{pl}), l/min	12
4	Powder flow rate Q_p, g/min	2.4
5	Speed of cooling liquid flow (for each circuit) Q_p, l/min	1.5
6	Thermal power released by constricted arc, W	840
7	Powder particle size, μm	100

Table 3 gives the technological parameters of the microplasma deposition process, used in modeling the operation of MPU-4 plasmatron with the nozzle

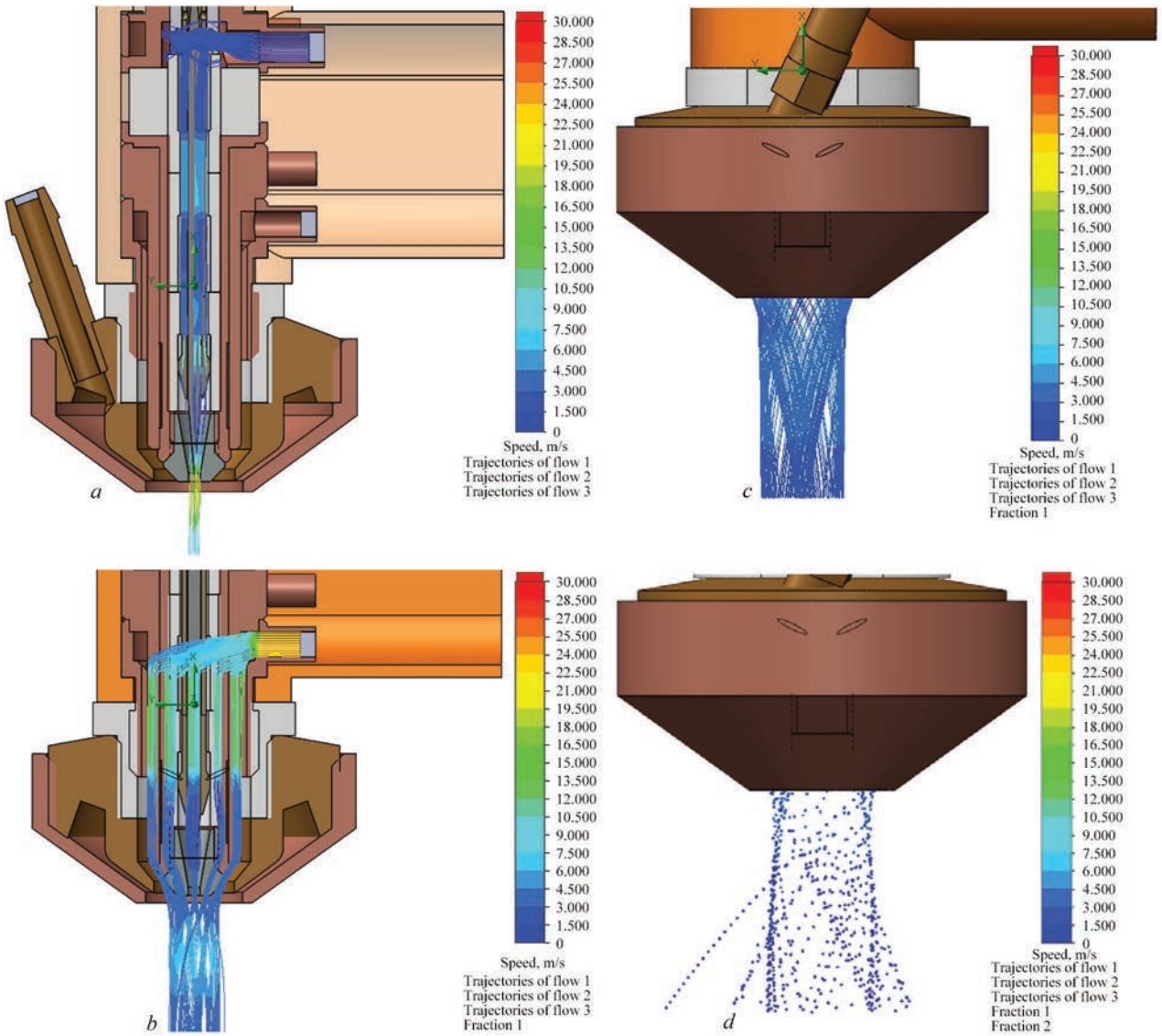

Figure 3. Speed and direction of gas flows in upgraded MPU-4 plasmatron: *a* — plasma-forming; *b* — shielding; *c* — transporting; *d* — powder particle flow

assembly for powder deposition. Modeling the gas dynamics allowed creation of an upgraded plasmatron design with satisfactory results for the flows of plasma-forming, shielding and powder transporting gases. Figure 3 shows the lines of plasma-forming, shielding and transporting gas flows and the flow of deposited powder particles. The design of the specialized nozzle assembly allowed achieving laminarity of the flows in the zones of the respective channels and at the plasmatron outlet.

Transverse templates were cut out of the samples produced by additive deposition and microsections were prepared to conduct metallographic analysis. After their grinding and polishing, electrolytic etching in chromic acid or ammonium sulphate was applied to reveal the microstructures [14]. Obtained structures of the samples were studied by the methods of optical (Neophot-30 microscope from Carl Zeiss, Germany) and analytical scanning electron microscopy (JSM-840 microscope from PHILIPS, Holland). Analytical scanning electron microscopy was applied to determine the chemical composition of the phases and metal grains (general and local point analysis). Optical microscopy was used to study the structural changes. Microhardness was measured with microhardness meter LM-400 (LECO series, USA) at 50 g load. Mechanical static tensile testing was conducted in an all-purpose tensile servohydraulic system MTS 810 (Material Test System, USA), using standard samples (GOST 6996–66) which were cut out of 3D printed walls across the deposited beads.

RESULTS OF TECHNOLOGICAL RESEARCH

Technological research was performed in keeping with the scheme given in Figure 4 [15]. The minimal wall thickness of the grown product in the conducted research on microplasma deposition was up to 3 mm. Investigations showed that during production of volumetric items by additive layer building-up by successive deposition, a very important parameter is the size of the built-up layer (deposited metal bead), as it determines the characteristics of the shape and the surface, as well as the precision of product formation. Therefore, a priority task, which was solved during selection of the deposition mode parameters, was determination of the best relationship between the flow of filler powder particles (Figure 3, *d*) and microplasma arc diameter. The difference in the conditions of deposition on the substrate and on the previously deposited bead was taken into account. In the latter case, when current is increased, the bead volume is reduced due to deterioration of the heat dissipation, penetration of the previous bead and increase of the pool length.

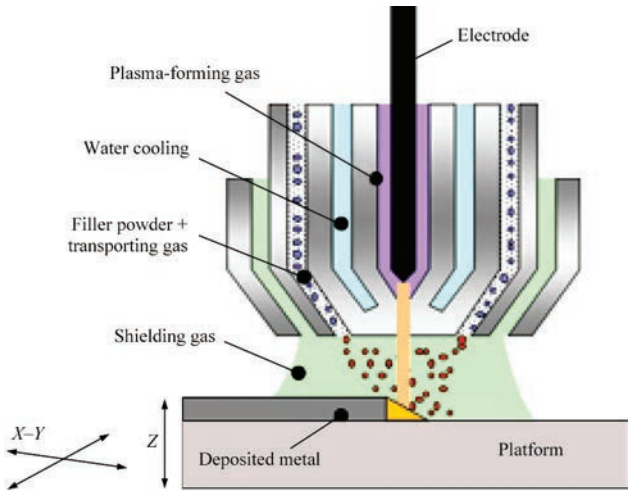

Figure 4. Scheme of conducting the technological research [15]

Another task, solved in order to select the mode, was increase in the fraction of useful filler powder consumption (UPC coefficient) during additive growing of the part. Experiments showed that the main cause for the powder filler losses is the movement of its dispersed particles on the periphery of the plasma arc column and further on their elastic reflection from the surface of the product being deposited, beyond the zone of the formed pool of deposited metal.

Thus, in case of realization of additive technology of growing thin-walled metal products with up to 3 mm wall thickness, it is important to be able to control such process characteristics, as concentration of the microplasma arc and addition of powder filler. In particular, in order to optimize the trajectories of filler material movement in the plasma arc, it is recommended to add filler powders to the arc at up to 40–45° to the plasmatron axis (Figure 2, *b*).

Research was performed with application of a microplasmatron with lateral distributed injection of the filler powder and diameters of plasma-forming nozzle channels d_{pl} = 1.8 and 2.5 mm and of focusing nozzle d_f = 2.5 mm and 4.5 mm (Figure 2, *b*). With these dimensions, its stable operation at welding current in the range of 5–50 A is ensured. The concentration of filler powder injection with flow rate G = 1.0 = 3.5 g/min through the microplasma arc to the anode plane (substrate, on which the first layer was deposited) was assessed by determination of the weight of powder, which penetrated into the weld pool, during successive increase of its dimensions. Width B of the molten metal pool (or deposited bead) changed with increase of welding current at a constant speed of microplasma arc movement in the range of 2–5 and 4–10 mm (Figure 5, Table 3). During the experiment, with gradual increase of the weld pool width by 5 times, dependencies of the change in the deposited bead specific mass M_d and UPC coefficient were derived which characterize the radial distribution of the filler powder.

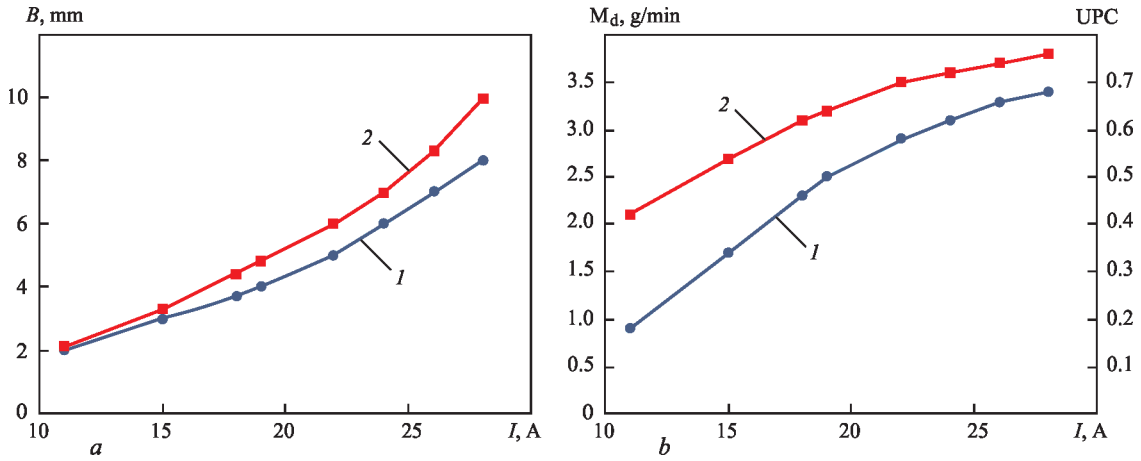

Figure 5. Dependence of bead width B (*a*), specific weight of deposited metal (HYF 103 alloy powder) M_d and UPC (*b*) on welding current I at deposition rate V = 3.24 mm/s: *1* — microplasmatron with d_{pl} = 2.5 mm, d_f = 4.5 mm, G = 3.2 g/min, B = 2–5 mm; *2* — d_{pl} = 1.8 mm, d_f = 2.5 mm, B = 4–10 mm

In keeping with the data in Figure 5, in order to produce volumetric products with up to 3 mm wall thickness (or with deposited bead width $B \leq 3$ mm), it is necessary to perform microplasma deposition at up to 15 A arc current. However, application of up to 30 A current is undesirable, because of the low process stability. To increase the stability, it is rational to increase the plasmatron arc current to 30–35 A, which requires increasing the deposition rate from 10–15 to 30 m/h to preserve the 3 mm wall thickness.

Further technological research was conducted with filler powder flow rate G = 3.0 g/min. The modes of additive microplasma deposition of the used powders were refined by the criteria of optimization of the deposited bead shape and formation of reliable fusion with the substrate and/or previous bead. The following main parameters of the deposition mode were selected: arc current I = 35 A, arc voltage U = 40 V, deposition rate V = 35 m/h (9.66 mm/s), energy input of deposition E = 87 J/mm (allowing for process efficiency of 0.6 [16]). Other parameters of the deposition mode are given in Table 3. Conducted research showed that in additive microplasma deposition with the selected powders (Table 1) the thickness of the deposited wall is preserved in the range of 3.0±0.3 mm with satisfactory stability (Figure 6). Here, the UPC coefficient is in the range of 0.84–0.88 (powder losses are equal to 16–12 %, respectively), which is an acceptable value.

RESULTS OF METALLOGRAPHIC STUDIES

In additive microplasma deposition complete melting of the powder occurred in all the cases of application of filler materials listed in Table 1. The deposited metal structure was characterized by a clearly expressed layering; deposited layer thickness was equal to 550–650 μm. Surfacing was performed in several passes, with successive deposition of the metal layers — one per pass. The structure of the fusion zones between the layers was homogeneous. The macrostructure of each deposited layer was homogeneous without formation of any defects, cracking or incomplete melting.

In case of application of powder of Ni–Cr–B–Si system for single-pass deposition, an equiaxed finely dispersed structure was produced in the deposited bead metal. The deposited material microstructure consisted of a two-phase matrix (Figure 7), in which a component prevailed, which appeared light when etching with hardness HV 4640–5720 MPa. Light-gray precipitates of higher hardness of HV 6030–7010 MPa are present alongside it (Figure 8). Thus, as a result of microplasma growing of the product, the microstructure of the heat-resistant nickel alloys consisted of a matrix of γ-solid solution (light-coloured), with intermetallic phases of the type of γ′-phase (Ni, Cr), (Al, Ti, Nb) and Ni(Cr, Mo, W) + carbides observed against its background. To increase the dispersion-hardening effect, these alloys, in the classical sense, should be heat treated. However, selection of the required temperatures and duration of holding during heat treatment of the innovative material produced by 3D layer-by-layer plasma deposition has not been performed so far. This can be the subject of further studies. No signs of overheating or burnout with a

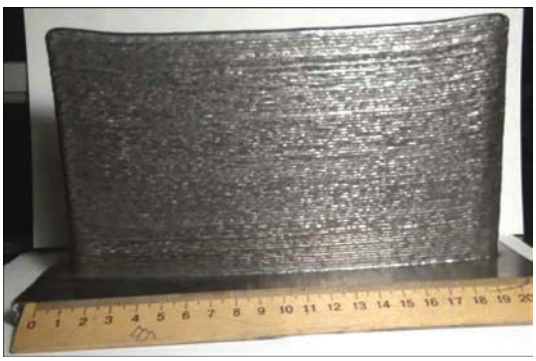

Figure 6. Appearance of a plate of metal produced by layer-by-layer microplasma deposition of HYF-103 powder

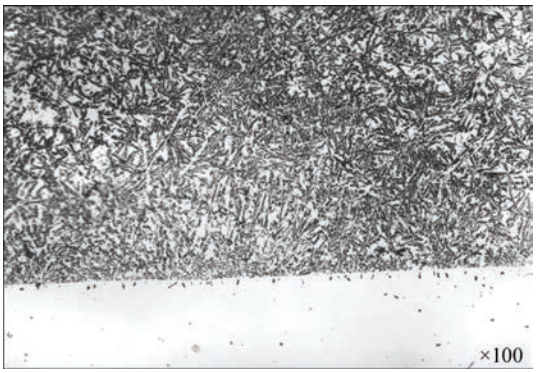

Figure 7. Structure of microplasma deposit, ×100

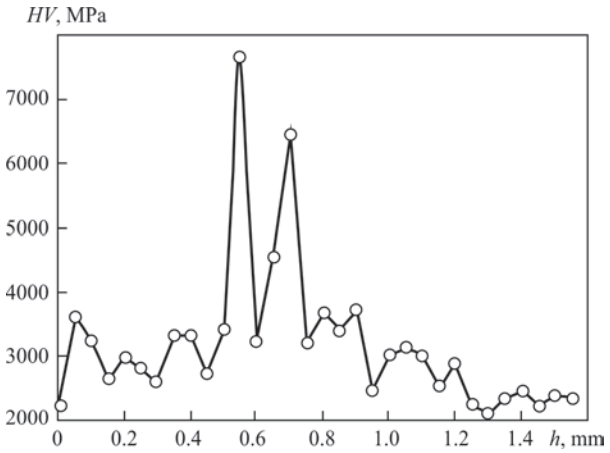

Figure 8. Distribution of microhardness $HV_{0.05}$, MPa with depth h, mm

jump-like increase in the grain size and intergranular melting were found in the microstructure of the grown samples.

Judging from the presence of peaks in the results of microhardness measurements and data of microstructural investigation, we can conclude that harder carbides of different shapes are included in the solid solution of the matrix. Strengthening phases had the shape of plates of different thicknesses, and their horseshoe-shaped and diamond-shaped precipitations were also found. The carbides were characterized by high hardness (HV > 20000 MPa). In addition to coarse (primary) carbides, their finer precipitates were also observed in the grown material matrix that, probably, promoted an increase in the strength and hardness of the material. Eutectic carbide precipitates of hardness on the level of HV 2340–3030 MPa are also observed over the entire deposit.

A thin light-coloured strip of hardness HV 2540–2860 MPa is also observed along the line of fusion with the base metal. This structural component is homogeneous along the entire length of the deposit, and its thickness is 10–12 μm. Note that the deposit structure is refined in the direction from the upper edge to the base metal of the substrate. Microanalysis of individual areas of the structure showed that the deposited metal composition is close to that of the deposited powder (see Table 1).

In case of application of HYF-103 powder for three-pass additive deposition, according to the data of electron microscopy, a fine dendritic structure of the deposited metal was produced, which contains both relatively large grains and fine ones. The large and fine dendrites form colonies, disoriented relative to each other (Figure 9). Crystals of different sizes were formed in the upper and lower parts of the sample, which resulted from the non-equilibrium conditions of solidification at microplasma 3D growing of the sample. So, in the lower part of the deposited metal the heat was removed through the base substrate, while in the sample upper part it was removed predominantly through thermal radiation and heat dissipation into the lower deposited layers. This resulted in slower cooling of the metal in the sample upper part and, thus, led to grain growth.

In the longitudinal direction the dendrites formed extended crystallite branches, oriented predominantly in the direction of heat removal and united into colonies. Microstructural analysis of the sample cut out in the lower part, showed that crystallite growth proceeds in one direction (Figure 9, *c*). The dendrites consist of grain blocks with similar crystal orientation, the boundaries of which were revealed as a result of etching. A comparison of the structure of metal in the samples, cut out in the longitudinal direction in the sample upper and lower parts, points to different nature of crystallization, during upward formation of the sample (Figure 9). Microanalysis in different individual sections of the structure showed that the depos-

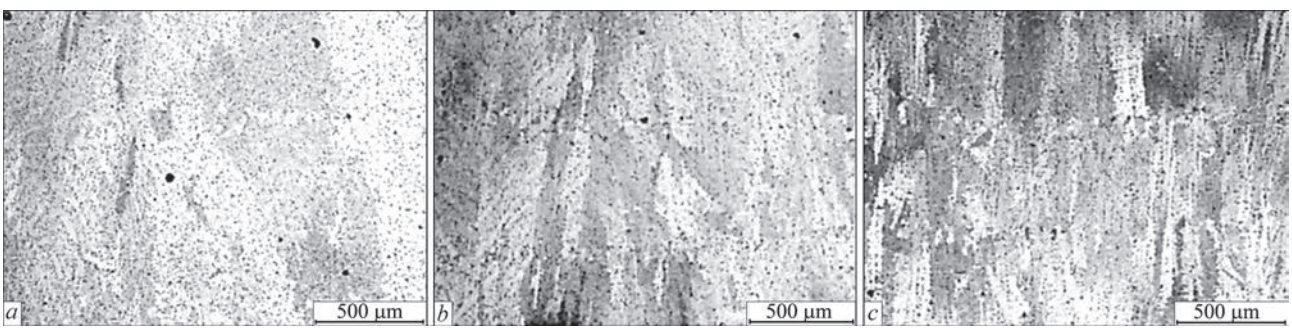

Figure 9. Microstructure of metal, produced by three-layer additive microplasma deposition of HYF-103 powder (×100): *a* — top of deposited sample; *b* — middle of deposited sample; *c* — bottom of deposited sample

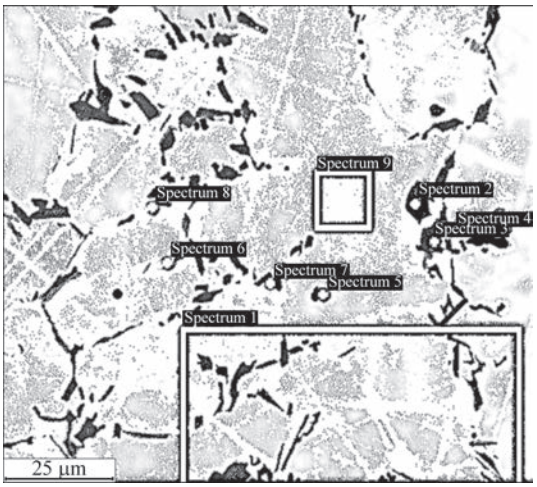

Figure 10. Microstructure of metal produced by additive microplasma deposition of HYF-103 powder, with indication of areas of element content microanalysis

ited metal composition is close to that of the deposited powder (Figure 10, Tables 1 and 4).

During examination in a reflected light optical microscope, the microstructure of samples of KhN50VMTYuB and KhN60VT alloys in the dendrite body appeared to be less homogeneous (Figure 11, *a*). Studying their structure in an electron microscope revealed that the dendrites of γ-solid solution have an internal structure with thin and intermittent boundaries of the block walls (Figure 11, *b*).

As one can see from the above microstructure, dispersion hardening during rapid cooling of the layers of microplasma deposited metal either did not occur, or occurred only to a minor extent.

DISCUSSION OF INVESTIGATION RESULTS

Conducted technological research showed that for the selected group of powders (see Table 1) the parameters of the mode of additive microplasma deposition predominantly depend on the fractional composition of the filler powder. Complete melting of the powder occurs under the conditions of application of microplasma deposition with the energy input of 85–90 J/mm and thermal power of ~800–900 W released by the constricted arc at additive growing of metal products. The metal structure is characterized by a clearly expressed layering; thickness of the deposited layer is equal to 500–650 μm.

Based on the results of the conducted technological research, it was determined that successive deposition of metal is manifested in formation of a relief on the sample side surface (Figure 6). Metal rolls are observed, which are an alternation of protrusions and depressions, caused, probably, by partial flowing of liquid metal down the side surface. Dimensions of these rolls approximately correspond to the height of the metal layer deposited in one pass. One of the ways to minimize this parameter is stabilization of additive microplasma deposition due to selection of its rational

Table 4. Element content in individual areas of the structure according to Figure 10

Spectrum	Chemical composition, wt.%												
	B	N	O	Mg	Si	V	Cr	Mn	Fe	Co	Ni	Mo	Total
1	–	–	–	–	0.95	–	16	0.31	72.16	0.32	9.1	1.17	100
2	–	–	–	–		–	49.26	–	47.38	–	1.12	2.24	100
3	–	–	–	–		0.24	48.64	–	48.09	0.4	0.91	1.72	100
4	–	–	17.41	9.17	8.85	–	9.37	–	48.21	0.41	6.06	0.52	100
5	20.25	19.63	–	–	0.26	–	7.85	0.32	45.51	0.28	5.09	0.81	100
6	–	–	–	–	0.65	0.41	15.52	–	56.74	0.4	6.47	19.8	100
7	–	–	–	–	0.67	0.26	17.15	–	59.99	0.44	6.64	14.85	100
8	–	–	–	–	0.72	0.25	14.86	–	61.16	0.31	7.41	15.28	100
9	–	–	–	–	0.95	–	13.68	–	74.64	0.36	9.79	0.58	100

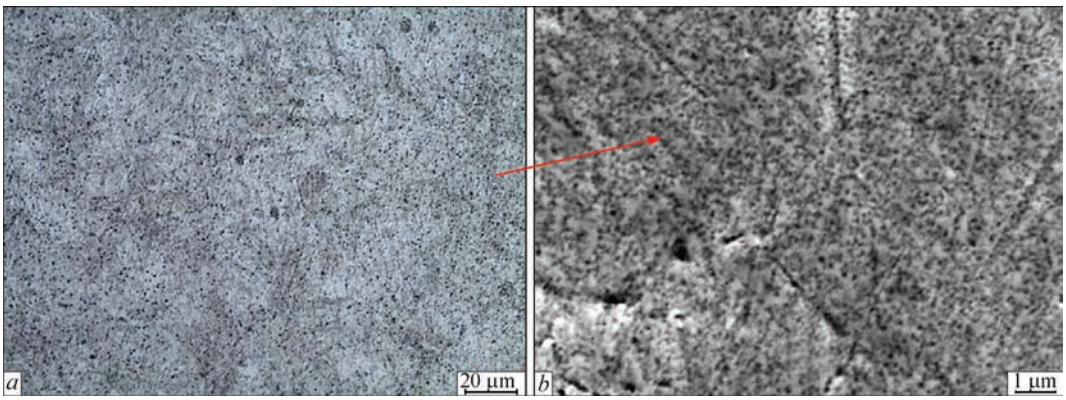

Figure 11. Microstructure of a sample, grown by microplasma deposition of KhN50VMTYuB alloy: *a* — ×500 (optical metallography); *b* — ×10 000 (electron microscopy)

Table 5. Mechanical properties of metal produced by additive microplasma deposition of HYF-103 powder

Sample number	F_0	L_0	L_k	σ_t, MPa	σ_y, MPa	δ, %
1	7.15	20.02	20.49	606	474	3.165
2	7.16	19.78	20.78	627	510	5.056
3	7.15	22.14	22.94	618	462	3.613
Averaged value	–	–	–	617	482	3.95

process modes. Another method to minimize this parameter is reduction of the height of the layer deposited in one pass. Such an approach, however, lowers the productivity of 3D printing of the product and requires individual optimization measures.

In multilayer microplasma deposition no such defects, as separation of the adjacent layers inside the deposit, because of incomplete fusion between the layers; molten material solidification in the form of spheres, and not a continuous layer; deformation through the difference in the coefficients of thermal expansion of the layers, were found. Fusion zones between the layers are not identified structurally, and a homogeneous structure is observed. The macrostructure of each surface-melted layer is quite homogeneous without formation of any defects, or cracking. The methods of optical and electron microscopy established that the sample metal structure is dendritic and contains both coarser and finer grains. Large and fine grains form colonies, disoriented relative to each other (for instance, Figure 8). Crystallite formation at successive deposition of the metal layers in the sample upper and lower parts is different, and it is determined by differences in the crystallization process. So, in the lower part of the deposited metal heat removal is more intensive, as it occurs through the base substrate, which has rather good heat conductivity. In the sample upper part heat removal is less intensive, as it is performed predominantly due to thermal radiation, while heat conductivity of the predeposited layer is due to the applied filler alloy, and it is predominantly low. This results in slower cooling of the metal in the sample upper part and, thus, leads to a certain grain growth.

Electron microscopy studies of phase composition of HYF-103 alloy layers, deposited by microplasma method in the selected rational mode showed trends of slight burnout of individual alloying components (Tables 1 and 4). So, manganese content decreased from 0.6 to ~0.3 wt.%. Boron burnout was also observed in individual sections. On the whole, however, reduction of the content of alloying components of the studied deposited alloys, is rather limited, and cannot be considered significant.

Ultimate strength σ_t, conditional yield limit $\sigma_{0.2}$ and relative elongation δ of the deposited metal at uniaxial tension were measured on samples 30 mm long, which were cut out along the vertical of a plate produced by layer-by-layer building up (see Figure 6). The deposited metal strength was assessed by the results of uniaxial tensile testing of three samples.

Conducted studies of mechanical properties (Table 5) allow us to conclude that the metal deposited by additive technology ensures rather high strength, reaching more than 600 MPa, where F_0 is the cross-sectional area of the sample; L_0 and L_k are the initial and final lengths of the sample; δ is the relative elongation.

Over the recent years the process of 3D printing of aircraft parts has become ever more relevant. Application of 3D printers significantly lowers the cost of the created products, increases the production flexibility and accelerates manufacture of the required repair kits of the parts. One of the most complicated tasks in this respect is 3D printing of metal parts, both finished and with additional machining. Application of additive microplasma deposition with metal powders for manufacture of 3D products for aviation equipment will allow a significant productivity improvement, compared to the currently available methods. So, application of microplasma deposition will allow reaching the productivity of ~3–4 kg/h, whereas laser deposition can provide the productivity of up to 1.5 kg/h. Moreover, microplasma deposition allows creating composite or functionally gradient metal layers, which will promote material saving, and will enable creating wear-resistant friction surfaces relative to a soft base during 3D printing. Equipment applied for microplasma deposition is much less expensive and easier to maintain, compared to laser equipment. On the whole, despite the need for final machining of critical functional surfaces, application of microplasma deposition can be regarded a promising direction of 3D printing of metal parts for aviation equipment. It is rational to focus further research on studying the influence of heat treatment on the structure and properties of products grown by innovative 3D microplasma deposition from heat-resistant nickel alloys, considered in the work.

CONCLUSIONS

1. It was determined that selection of the mode of additive microplasma deposition of the chosen group of iron- and nickel-based powders is predominantly due to filler powder granulation. At additive microplasma growing of metal products with up to 3 mm wall thickness with application of Fe- and Ni-based powders with fraction size of 40–100 μm complete melting of the powder occurs in the modes, ensuring the energy input of 85–90 J/mm with thermal power of ~800–900 W released by the constricted arc.

2. It was established that the metal structure in samples produced by microplasma deposition, consists of dendrite colonies disoriented one relative to another, which contain both relatively large and finer grains. In the deposited metal lower layer small-

er-sized crystallites are formed, due to more intensive heat removal through the steel substrate of the base. In the upper layers of the deposited metal larger-sized crystallites are formed, owing to reduction in the heat removal intensity, which is promoted by application of filler alloys with rather low heat conductivity.

3. Mechanical testing for static tension of samples cut out of the deposited metal across the deposited beads showed that the strength of HYF-103 alloy exceeded 600 MPa at yield limit values higher than 480 MPa and relative elongation close to 4 %. Such results are attributable to absence of deposition defects and small fraction of burning out of the deposited metal alloying elements.

4. Conducted research showed the fundamental possibility of formation of dispersed dendritic structures with grains of different spatial orientation, structural homogeneity of the deposited layers without clearly expressed fusion zones, and absence of pores or cracking. Such trends of structure formation are indicative of the good prospects for further application of additive microplasma deposition for 3D printing of parts from iron- and nickel-based corrosion- and heat-resistant alloys, in particular, parts of aerospace engines.

REFERENCES

1. Moon, S.K., Tan, Y.E., Hwang, J., Yoon, Y.-J. (2014) Application of 3D printing technology for designing light-weight unmanned aerial vehicle wing structures. *Inter. J. of Precision Eng. and Manufacturing-Green Technology*, **1**, 223–228. DOI: https://doi.org/10.1007/s40684-014-0028-x
2. Chee, K.C., Kah, F.L., Chu, S.L. (2010) *Rapid prototyping: Principles and applications*. 3rd Ed. World Scientific Publ. Co Pte Ltd. DOI: https://doi.org/10.1142/6665
3. Martinez, D.W., Espino, M.T., Cascolan, H.M. et al. (2022) A comprehensive review on the application of 3D printing in the aerospace industry. *Key Eng. Materials*, **913**, 27–34. DOI: https://doi.org/10.4028/p-94a9zb
4. Singamneni, S., Lv, Y., Hewitt, A. et al. (2019) Additive manufacturing for the aircraft industry: A review. *J. of Aeronautics & Aerospace Eng.*, 8(**1**), 214. DOI: https://doi.org/10.35248/2168-9792.19.8.215
5. Gadagi, B., Lekurwale, R. (2021) A review on advances in 3D metal printing. *Materials Today: Proceedings*, 45(**1**), 277–283. DOI: https://doi.org/10.1016/j.matpr.2020.10.436
6. Matthews, N. (2018) Chapter fifteen — Additive metal technologies for aerospace sustainment. *Aircraft Sustainment and Repair*, **2018**, 845–862. DOI: https://doi.org/10.1016/B978-0-08-100540-8.00015-7
7. Gisario, A., Kazarian, M., Martina, F., Mehrpouya, M. (2019) Metal additive manufacturing in the commercial aviation industry: A review. *J. of Manufacturing Systems*, **53**, 124–149. DOI: https://doi.org/10.1016/j.jmsy.2019.08.005
8. Yamazaki, T. (2016) Development of a hybrid multi-tasking machine tool: Integration of additive manufacturing technology with CNC machining. *Procedia CIRP*, **42**, 81–86. DOI: https://doi.org/10.1016/j.procir.2016.02.193
9. Peleshenko, S., Korzhyk, V., Voitenko, O. et al. (2017) Analysis of the current state of additive welding technologies for manufacturing volume metallic products (Review). *Eastern-European J. of Enterprise Technologies*, 3–1(**87**), 42–52. DOI: https://doi.org/10.15587/1729-4061.2017.99666
10. Kumar, P., Jain, N.K. (2020) Effect of material form on deposition characteristics in micro-plasma transferred arc additive manufacturing process. *CIRP J. of Manufacturing Sci. and Technol.*, **30**, 195–205. DOI: https://doi.org/10.1016/j.cirpj.2020.05.008
11. Wang, H., Jiang, W.H., Valant, M., Kovacevic, R. (2003) Microplasma powder deposition as a new solid freeform fabrication process. *Proc. of the Institution of Mechanical Eng., Pt B: J. of Eng. Manufacture*, 217(**12**), 1641–1650. DOI: https://doi.org/10.1243/095440503772680578
12. Ovchinnikov, O.V., Duryagina, Z.A., Romanova, T.E. et al. (2021) *Powder titanium alloys for additive technologies: Structure, properties, modeling*. Kyiv, Naukova Dumka [in Ukrainian].
13. Rezydent, N., Stepanova, N. (2023) Using the solid works flow simulation CFD package to study the performance indicators of the cyclone-utilizer. *Modern Technology Materials and Design in Construction*, 33(**2**), 192–197. DOI: https://doi.org/10.31649/2311-1429-2022-2-192-197
14. Akca, E., Trgo, E. (2015) Metallographic procedures and analysis — A review. *Periodicals of Eng. and Natural Sci. (PEN)*, 3(**2**), 9–11. DOI: https://doi.org/10.21533/pen.v3i2.51
15. Korzhyk, V., Gao, S., Khaskin, V. et al. (2024) Features of the stress-strain state of 3D metal objects produced by additive microplasma deposition of the powder of a Fe–Cr–Ni–B–Si system. *Applied Sci.*, **14**, 4159. DOI: https://doi.org/10.3390/app14104159
16. Sidharth, Rana R., Pandey S. (2023) Configuring microplasma for material process optimization. *Materials Today: Proceedings*. DOI: https://doi.org/10.1016/j.matpr.2023.01.339

ORCID

V.Yu. Khaskin: 0000-0003-3072-6761,
K.M. Sukhyi: 0000-0002-4585-8268,
O.V. Ovchynnykov: 0000-0001-5209-7498,
O.V. Zaichuk: 0000-0001-5209-7498

CONFLICT OF INTEREST

The Authors declare no conflict of interest

CORRESPONDING AUTHOR

V.Yu. Khaskin
E.O. Paton Electric Welding Institute of the NASU
11 Kazymyr Malevych Str., 03150, Kyiv, Ukraine.
E-mail: khaskin1969@gmail.com

SUGGESTED CITATION

V.Yu. Khaskin, K.M. Sukhyi, O.V. Ovchynnykov, O.V. Zaichuk (2025) Application of microplasma deposition for 3D printing of aerospace engine parts. *The Paton Welding J.*, **4**, 12–21.
DOI: https://doi.org/10.37434/tpwj2025.04.03

JOURNAL HOME PAGE

https://patonpublishinghouse.com/eng/journals/tpwj

Received: 05.03.2025
Received in revised form: 24.03.2025
Accepted: 08.05.2025